Available online at www.sciencedirect.com
SCIENCE DIRECT®
Marine Geology 204 (2004) 145–159
MARINE GEOLOGY
INTERNATIONAL JOURNAL OF MARINE GEOLOGY, GEOCHEMISTRY AND GEOPHYSICS
www.elsevier.com/locate/margeo

A new 'schlieren' technique application for fluid flow visualization at cold seep sites

V. Karpen [a,b,*], L. Thomsen [a], E. Suess [b]

[a] International University Bremen, P.O.Box 750561, 28725 Bremen, Germany
[b] GEOMAR, Research Center for Marine Geosciences, Wischhofstr. 1–3, 24148 Kiel, Germany

Received 25 June 2002; received in revised form 20 October 2003; accepted 4 December 2003

Abstract

A new optical instrument for the investigation of submarine fluid flows based on a 'schlieren' technique was developed and successfully deployed at cold seep sites. With this application it is possible to visualize the discharge and distribution of fluids in the ambient bottom water and to resolve microstructures and mixing processes at a scale of centimeters. The system is sensitive to small refractive index anomalies caused by temperature and salinity variations. Density anomalies of $\Delta\sigma_t = 0.049$ are detectable evaluated by in-situ temperature variations of $\Delta T = 0.1$°C and salinity variations of $\Delta S = 0.045$ psu. In flume experiments the smallest detectable density variation was even lower with $\Delta\sigma_t = 0.023$. The technique has been successfully applied in two different environments. First field experiments were performed to observe submarine groundwater discharge in Eckernförde Bay (western Baltic Sea) at shallow water depths. Subsequently, the 'schlieren' technique was successfully brought to a cold seep location at the Cascadia convergent margin (800 m water depth). The discharge of fluids was recorded in both field experiments which enabled a qualitative seep site identification.

Keywords: seepage; submarine springs; groundwater; flowmeters; 'schlieren'; visualization

1. Introduction

Fluid venting is a widespread phenomenon in a variety of different environments and in many parts of the world's oceans. Seeps occur at active and passive margins from the tidal zone to trench-depths of more than 8000 m (Paull et al., 1984; Suess et al., 1985; Kulm et al., 1986; Hovland, 1992; Wallmann et al., 1997a; Suess and Linke, 2002). The main focus of recent investigations has been the fluid discharges at hot vents, cold seeps, and groundwater seeps in near-shore areas. It is known that all of these environments are directly influenced by fluid flux from the geosphere (Corliss et al., 1979; Aharon, 1994; Moore, 1996). Flow rates reported so far vary over several orders of magnitude (<0.1 mm yr^{-1} to >1000 m yr^{-1}; Tryon et al., 2001) and highest fluxes in order of cubic meters per second are known from springs at karst regions off Mediterranean coasts like Sicily and Greece. Vent sites at accre-

* Corresponding author. Fax: +49-421-200-3229.
E-mail addresses: v.karpen@iu-bremen.de (V. Karpen), l.thomsen@iu-bremen.de (L. Thomsen), esuess@geomar.de (E. Suess).

0025-3227/03/$ – see front matter © 2003 Elsevier B.V. All rights reserved.
doi:10.1016/S0025-3227(03)00370-0

tionary ridges are characterized by a unique benthic community, massive occurrence of authigenic carbonates, and methane hydrate (Suess et al., 1999). Submarine groundwater discharges in coastal zones have been documented since the 19th century (Sonrel, 1868). It is known that they occur as springs and seeps in near-shore areas (Hovland and Judd, 1988). Submarine springs, for example, are described for many locations around the world such as from the Gulf of Mexico (Cable et al., 1996), both Florida coasts (Corbett et al., 1999), the Mid-Atlantic Bay (Moore, 1996), western Australia (Johannes and Hearn, 1985), and the Baltic Sea (Whiticar and Werner, 1981).

However, the environmental implications for the coastal zones have only been recognized recently (Burnett et al., 2001). At the continental shelves, groundwater is transported down-gradient through artesian aquifers, even over long distances, and recent studies have estimated the maximum discharge rates to be as as high as 10% of the global river flow (Zektser and Loaiciga, 1993). Investigations over the past few decades have revealed that the groundwater discharge, at least in some cases, may be important for geochemical budgets and may cause ecological effects (Johannes, 1980; Valiela et al., 1990). These submarine groundwater discharges are often responsible for the influx of nutrients causing the formation of plankton blooms (LaRoche et al., 1997). Herbicides and pesticides may also find their way into the marine environment by that route. Thus, it appears that anthropogenic pollution via submarine groundwater discharge has to be seriously taken into account (Burnett et al., 2001).

Groundwater seeps forming pockmarks in the Eckernförde Bay have been known since the early works of Whiticar and Werner (1981). During the following years, the Eckernförde Bay became an important study area for near-coastal groundwater discharges addressing issues such as salinity and temperature anomalies, source depth, periodicity of flow and above all flow rates (Albert et al., 1998; Bussmann and Suess, 1998; Bussmann et al., 1999; Sauter et al., 2001; Whiticar, 2002).

In order to quantify submarine fluid flow, different approaches have been developed like modeling, direct measurements, and tracer techniques. The 'seepage meter', first described by Lee (1977), represents a direct measurement of released fluids with the use of a defined cylinder penetrated into the sediment. The same approach in principle was used for new instruments developed by Linke et al. (1994) and Tryon et al. (2001). Area wide investigations covering the influence of seeps within a bay or a coastline are performed with tracer techniques (Carson et al., 1990). However, the determination of fluid discharges is still difficult because of highly variable rates (Tryon and Brown, 2001) as well as a large spectrum of magnitudes of rates. Focused fluid flow along fault traces and other geological features such as pockmarks, fault displacements, and outcrops of sedimentary strata are known as diffuse flow through sedimentary sequences (Aharon, 1994).

The direct measurement of flow rates always produces artefacts due to the presence of a flow chamber whereas tracer techniques only provide area wide information of seepage activities. For a localized observation without enclosing the sediment there is no application so far but one is needed for an accurate description of active seep sites. A new optical approach to detect and investigate fluid flow at cold seep settings is presented here. The system is based on a 'schlieren' technique first described by Töpler (1866). The technical setup of the In-situ 'schlieren' Technique Application (ISTA) will be presented below, followed by results from laboratory tests and first field deployments.

2. Instrumentation

2.1. The 'schlieren' technique

The term 'schlieren' describes gradient disturbances of inhomogeneous transparent media (Töpler, 1867; Schardin, 1942). The disturbance is due to relatively small refractive index differences within the overall background. By definition, optical inhomogeneities bend light rays in any direction other than the 'normal' direction (Settles, 2001). 'Schlieren' objects occur in solids, liquids, and gases. They may result from temper-

ature changes, high-speed flows, or the mixing of materials with dissimilar refractive indices. The 'schlieren' technique is based on the angular deflection of a light ray when it passes through a fluid region characterized by refractive index inhomogeneities. These inhomogeneities are generally caused by density variations; in the marine environment primarily by salinity and temperature anomalies. For most investigations in the marine environment, variations in the seawater refractive index n are negligible and a constant value of $n \approx 4/3$ is given (Dietrich et al., 1975). The refractive index of a medium $n = c_0/c$ is defined by the speed of light in a vacuum $c_0 = 3 \times 10^8$ m s^{-1} in relation to the speed in the medium c. The refractive index of seawater is dominated by salinity and temperature as is its density (Fofonoff and Millard, 1983). The index increases with increasing salinity and decreasing temperature. It is well known, that there exists a close relationship between refractive index n and density ϱ, which is expressed by the Lorentz–Lorenz equation, where r is the specific refraction:

$$\varrho = \frac{1}{r} \cdot \frac{n^2 - 1}{n^2 + 1} \tag{1}$$

A more accurate attempt to define a density vs. index of refraction algorithm with respect to temperature, salinity, and pressure variations was presented by Seaver (1985) and Millard and Seaver (1990). For the new in-situ 'schlieren' instrument described here, a Z-type 'schlieren' system (Schardin, 1942) was developed, which represents the most commonly used arrangement for various experimental setups in optical physics. This experimental setup consists of a light source, two spherical mirrors, and an observation unit arranged in the form of the letter Z as shown in Fig. 1.

All 'schlieren' methods require a light beam from a point source, mirrors (or lenses), and knife-edges or some other device to block off the refracted light. In order to obtain a very sensitive application, an optical pathway with two knife-edges was designed. To produce a one-sided sharply limited point source, the emitted light is focused by the first lens on a knife-edge. This semi-circular image interacts with the second knife-edge in front of the camera. The light beam is collimated by the first spherical mirror to form parallel light rays, where the test section is located. The second mirror refocuses the light on the knife-edge located in front of the camera. The semi-circular image of the light is again formed in this layer. Transparent 'schlieren' objects are barely imaged without this second edge. 'Schlieren' objects cause angular deflection of light rays due to their different refractive indices, symbolized by the dashed lines in Fig. 1. The existence of the second knife-edge, blocking almost 50% of these deflected rays, makes the 'schlieren' objects visible. A finite 'schlieren' object refracts many such rays in many directions. All rays are

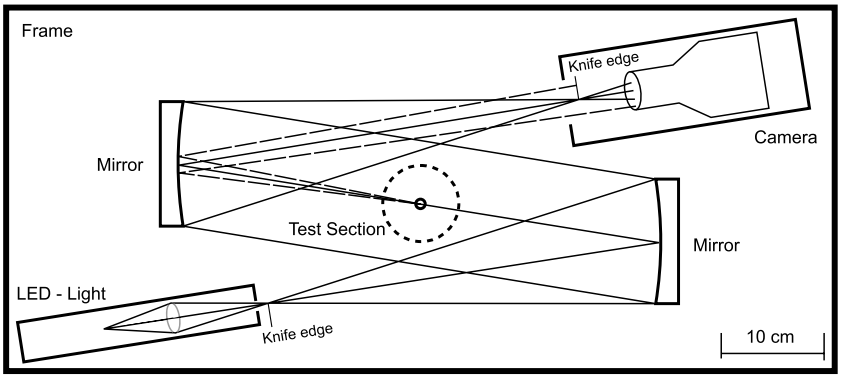

Fig. 1. 'Schlieren' system (top view) with light source, spherical mirrors, and camera. Any disturbance, such as a discharged fluid with a different refractive index, causes an angular deflection of light rays – symbolized by the dashed lines, whereby almost 50% of the rays are filtered out by the knife-edge of the camera.

blocked by the knife-edge, leaving dark corresponding image points against a bright background. Refracted rays passing the knife-edge brighten image points on the screen. Eventually the sum of these deflected rays image a picture of the 'schlieren' object which is accentuated by a brightened and a shadowed side. In practice, the knife-edge used is an ordinary razor blade. For the second edge, the ring of an ancillary lens was adapted. The lens was removed, the blade integrated, and affixed in front of the camera. The optical pathway ends at the CCD camera, which is focused and zoomed on the test section. The visible area is approximately 6×6 cm. The field of view is located at a height of 12 cm above bottom. The desired sensitivity is attained by adjusting the two knife-edges. The formation of parallel light within the test section enhances the sensitivity compared to other 'schlieren' setups. In contrast to the use of lenses, mirrors have an important advantage. They generate the same optical pathway in air as they do in water. This is a major demand on the new instrument because precise adjustments of the optical pathway have to be done on board ship prior to deployment. There is no pressure housing necessary to cover the optical pathway as needed for a shadow-graph technique with the use of lenses (Converse et al., 1986). This reduces the weight and the cost of the instrument. In Table 1 the specific components and brands used are listed.

All components were constructed for deep-sea deployment. Thus, an autonomous deep-sea lamp was also developed (Fig. 2). To allow long deployment times an LED light source with a minimal energy requirement was selected. The emitted light is captured by a 35-mm lens and focussed on the first knife-edge located at the front of the pressure housing. For the required precise setup, the LED and the lens were attached to two metal bars and thus they were continuously adjustable.

For some of the field studies an inverted funnel was integrated into the test section to better focus the flow. When the system is deployed over a potential vent site, the funnel is placed directly on the sediment surface. The smaller exhaust port at the top is visible on the video screen. Escaping fluids are channeled through the funnel and are visible as 'schlieren' objects as long as their refractive index is different from that of ambient bottom water. Fluids escaping from around the funnel are also detectable. They appear as diffuse outflow patterns in the background. For deep-sea deployments, the ISTA was integrated into a frame which was designed to fit into the frame of a TV-guided multiple-corer (Barnett et al., 1984). The CCD-camera is a commercial system, a Yashica KX-V1 Hi8 Video Camera Recorder with an optical resolution of 500 000 pixels cm^{-2} and an Aanderaa pressure housing (Thomsen et al., 1996). The time lapse controller allows the tester to bridge the time gap until a qualified location is selected. The video tapes are analyzed with image processing software (NIH Image 1.62). In this way the fluid discharge could be characterized. During deployments in the Baltic Sea, the ISTA was additionally equipped with a CTD (Table 2) to gain more information about the heterogeneity of the water masses. The sensors were located approximately 30 cm away from the test section.

Table 1
ISTA components, Z-type

Component	Specification
Mirrors	Edmund Scientific, spherical, ∅ = 152.4 mm, f = 609.6 mm, λ/4
Camcorder	Yashica KX-V1 Hi 8
Camera housing	Aanderaa, O.D. = 129 mm, I.D. = 115 mm, 600 bar
LED	∅ = 5 mm, 20 mA
Power supply	Three A-size batteries
Lens	35 mm
Light housing	O.D. = 60 mm, I.D. = 40 mm, 600 bar
Funnel	Bottom ∅ = 114 mm, top ∅ = 5.8 mm
Timer	VCR-Timer for Sony, Yashica camcorder

Table 2
FSI 3″ Micro CTD, Falmouth Scientific, Inc., datalogging capability, sample rate 1.83–4.5 frames per second

Parameter	Conductivity	Temperature
Sensor	Inductive cell	Platinum thermometer
Range	0–7.0 S/m	−2° to 32°C
Accuracy	±0.0002 S/m	±0.002°C
Resolution	0.00001 S/m	0.0001°C
Response	5.0 cm at 1 m/s flow	150 msec

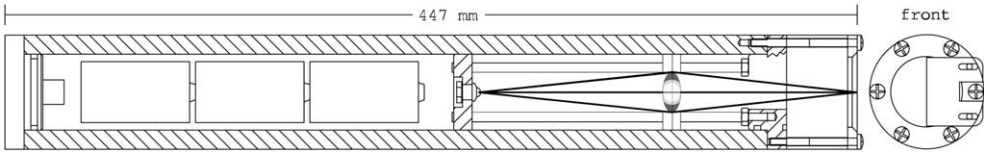

Fig. 2. LED light source. The light source is a standard yellow LED. The power supply is provided by three A-size batteries. A 35-mm lens is integrated into the pressure housing. The emitted light is focused on a knife-edge located at the front of the lamp.

2.2. Flume testing

To determine the sensitivity of the optical system with regard to temperature and salinity anomalies, a series of experiments was carried out in the GEOMAR seawater flume (Karpen, 1999; Springer et al., 1999). The tests were performed to define the limit to which temperature and salinity in different heterogeneous water mixtures are detectable and how discharged fluids with variable buoyancy behave under current conditions. For the experiments, an optical setup was built around the flume. A trough filled with a 10-cm sand layer was integrated into the test section. To discharge water of different density through this layer, tubes were introduced from the outside of the flume to the bottom of the sediment layer. For investigation of the focussed fluid flow, a nozzle was attached to the sediment surface which captured the ascending fluid. Its diameter at the base was 8 mm and the outlet diameter was 4 mm. To determine the influence of horizontal bottom current condition, the nozzle was removed and the undisturbed discharge through the sediment was recorded. Temperature anomalies as low as $\Delta T = 0.2$°C between ambient and discharged water could be clearly visualized (Fig. 3). A density difference of $\Delta\sigma_t = 0.023$ is calculated according the algorithms of Fofonoff and Millard (1983), with $\Delta\sigma_t = (\varrho - 1) \times 10^3$.

The experiments were repeated for salinity anomalies. A positive salinity anomaly is shown in Fig. 4. Due to its higher density, the fluid first ascends but then cascades down and stratifies at the sediment surface. In the experimental setup, salinity anomalies as low as $\Delta S = 0.2$ psu corresponding with a variation of the density $\Delta\sigma_t = 0.156$, were still readily detectable. Knowing the results of the temperature experiments, it is possible to calculate the theoretically smallest detectable salinity variations. Due to temperature anomalies of $\Delta T = 0.2$°C the density variation of $\Delta\sigma_t = 0.023$ was determined. With this value it is possible to determine the theoretical value for the detectable salinity variations which is $\Delta S = 0.03$ psu.

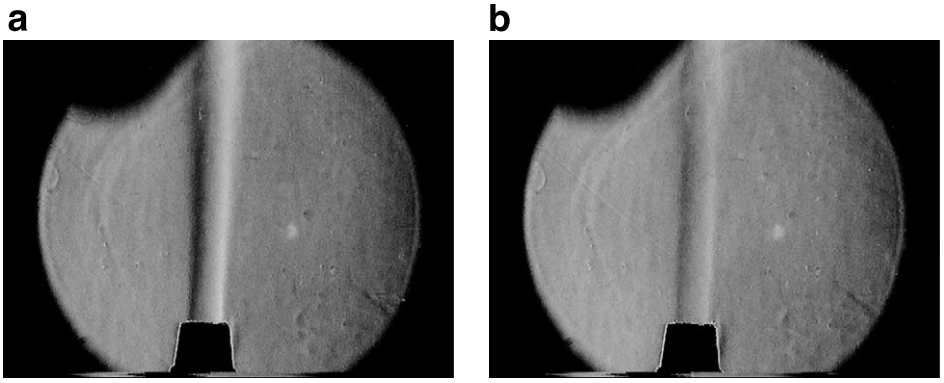

Fig. 3. Discharge of fluid into the ambient water under no-current conditions. (a) The discharged fluid has a positive temperature anomaly of $\Delta T = 2.4$°C. (b) The jet is still visible at a temperature difference of as little as $\Delta T = 0.2$°C. The horizontal diameter of each image is about 5 cm.

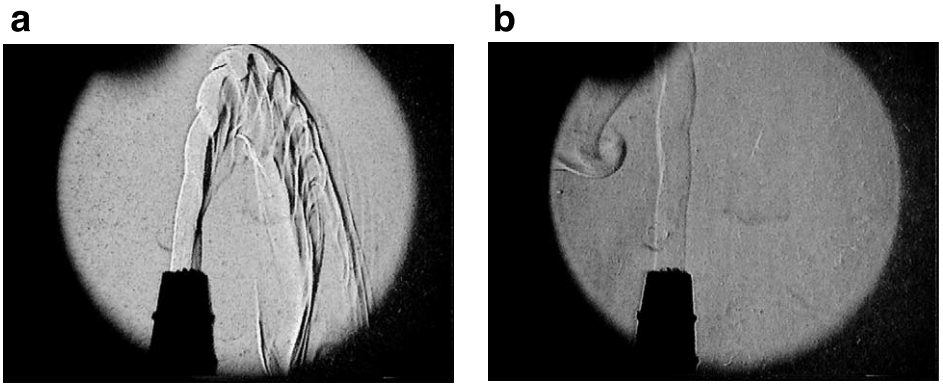

Fig. 4. A discharge of a more saline fluid into the ambient water under no-current conditions. (a) The discharged fluid has a positive salinity anomaly of $\Delta S = 2.4$ psu. (b) The salinity difference is just $\Delta S = 0.2$ psu and still the discharged fluid is easily recognized. The horizontal diameter of one image is about 5 cm.

For the field studies, it was important to consider how discharged fluids behave in the presence of a turbulent bottom boundary layer and hence appropriate tests were conducted. Fig. 5 shows the discharge of a less dense fluid from the sediment into a denser fluid layer. Without the influence of a current (Fig. 5a), the fluid ascends more or less vertically. The second image (Fig. 5b) shows the effect of a horizontal current with a free flow velocity of 2 cm s^{-1}. The fluid is captured in the turbulent bottom layer and small eddies and microstructures are visible.

The experiments demonstrate that the discharged fluids do not homogenize and mix immediately but rather are inserted into the ambient bottom water and retain their properties for a while. These results emphasize the strength of the technique because the cold seep environments are continuously influenced by a fluid flow which is difficult to detect and to survey. The capability of the new instrument to visualize and image small-scale mixing processes is an important attribute for field studies.

3. Field deployment

The new ISTA was tested in two different ma-

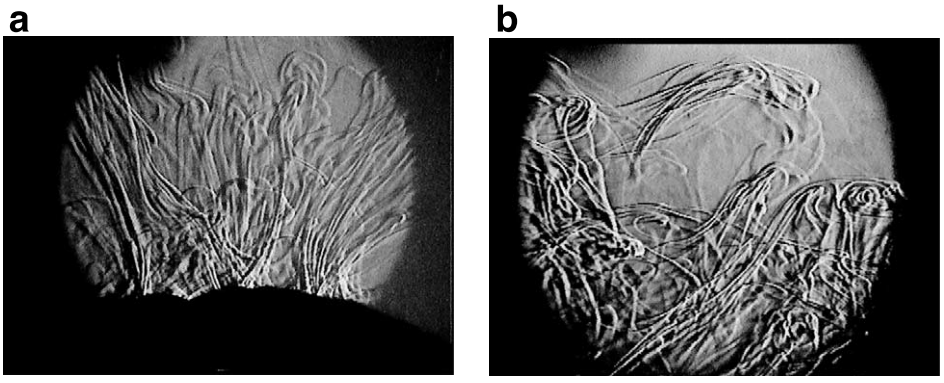

Fig. 5. Influence of current conditions of a discharged less dense fluid. (a) Discharge ($\Delta S = 1$ psu) without current is simulated with a detailed view of the sediment-water interface. (b) Discharge ($\Delta S = 17$ psu) with a current velocity of 2 cm s^{-1}. The horizontal diameter of each image is about 5 cm.

rine environments. Groundwater seepage was monitored in the Eckernförde Bay (western Baltic Sea) and a cold seep ecosystem at Hydrate Ridge was used as an offshore test at a water depth of 776 m.

3.1. Eckernförde Bay, Baltic Sea

Elongated and horseshoe-shaped shallow depressions in soft surface sediments of Eckernförde Bay have been known as sites of groundwater discharge since the echo-sounder profiles of Werner (1978) and Whiticar and Werner (1981). Based on these and subsequent investigations, the 'schlieren' technique camera system was deployed in and around these pockmarks (Khandriche and Werner, 1995; Bussmann and Suess, 1998; Sauter et al., 2001). The freshwater-induced pockmarks were located with the echo-sounding system aboard RV *Littorina* (Institut für Meereskunde, Kiel, Germany). The vessel was equipped with an echo-sounder *ELAC* LAZ 4700 with 30 and 200 kHz. The different deployment locations are shown in Fig. 6.

Measurements were performed at eight stations (Table 3) in water depths ranging from 5 to 25 m. Two of these deployments were placed intimately within a pockmark location. However, due to the very soft sediments and strong sediment resuspension, optical measurements were not possible within the pockmarks. In the following, the data gathered at Stations 2, 4 and 6, will be discussed in detail.

Table 3
Stations, Eckernförde Bay

Station No.	Latitude (North)	Longitude (East)	Depth (m)
1	54°28.961	10°02.539	10.8
2	54°28.904	10°01.969	6.7
3	54°28.850	10°01.709	10.3
4	54°30.251	10°01.712	18.6
5	54°30.243	10°01.203	24.7
6	54°30.443	10°02.387	7.9

3.1.1. Lateral transport of discharged water masses

In the screen shots compiled in Fig. 7, the influence of discharged groundwater is easily visible. At 6.7 m water depth (Station 2), the bottom water first appeared to be clear and undisturbed (Fig. 7a). Later during the experiment, another water mass entered the field of view due to the bottom current (Fig. 7b–d). This water mass was clearly visible by the "schlieren" objects caused by the different refractive index values. The bottom flow velocity was determined by simultaneously tracking suspended particles in the flow (Thomsen et al., 1996). During this video sequence, the velocity was about 5 cm s^{-1}, oriented from right to left. In Fig. 7d, a small eddy is visible. Its diam-

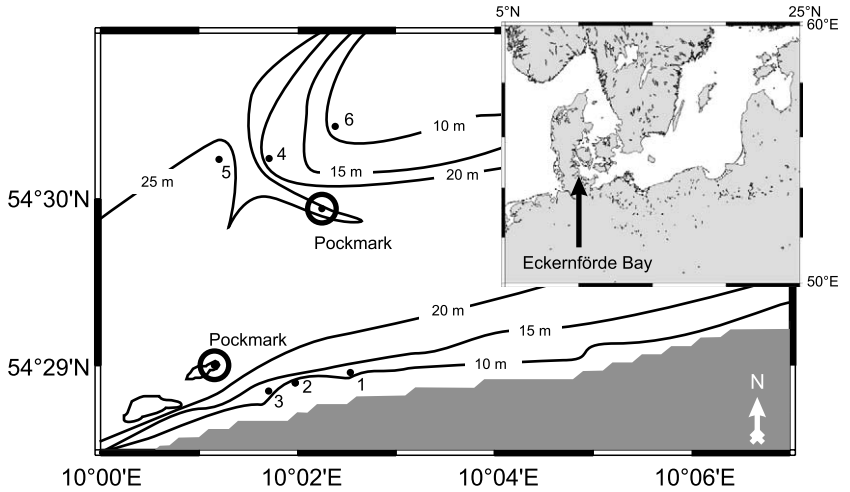

Fig. 6. Research area in the Eckernförde Bay with station locations (dots with numbers) and isobaths.

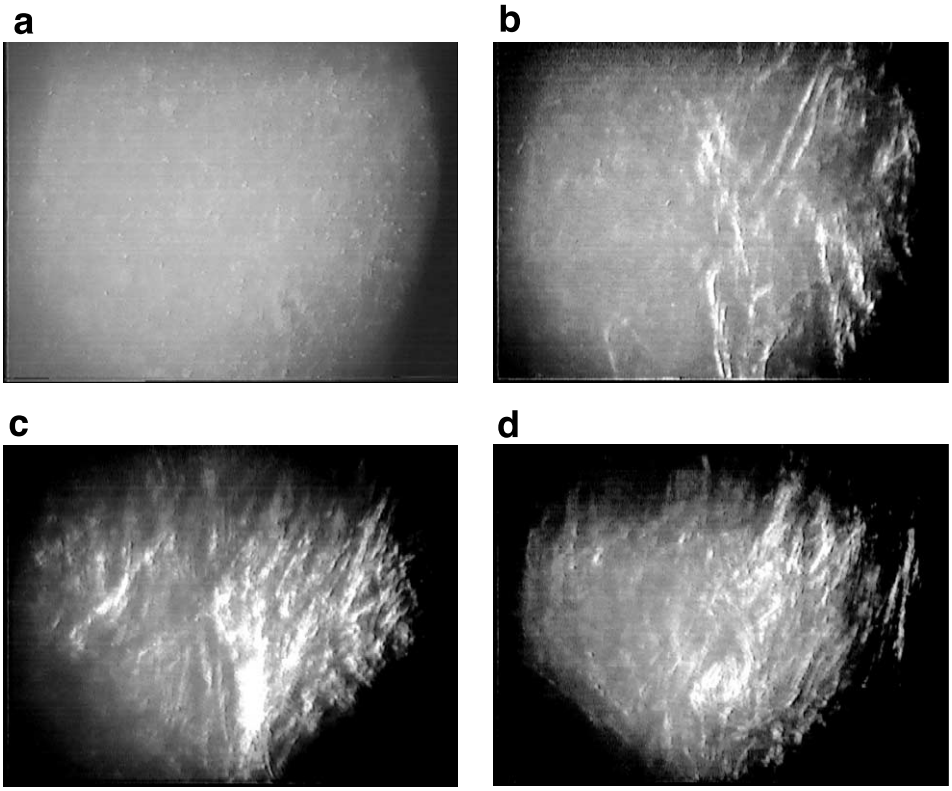

Fig. 7. Station 2, 6.7 m water depth. Horizontal fluid flow is visualized in this video sequence. The first image (a) shows the undisturbed bottom water. In the next images (b–d) the propagation of a discharged fluid into the field of view can be seen. The diameter of each image is about 6 cm. The elapsed time between the first and the last image is approximately 5 s. The bottom current velocity is about 5 cm s^{-1}. The current direction is from right to left.

eter is less than 1 cm and shows that even such microstructures are easily resolved and visualized.

During the following deployments, a CTD was aligned with the ISTA to gain more information about the physical properties of the different water masses. The CTD data and screen shots from Station 6 at 7.9 m water depth are shown in (Fig. 8). For an accurate illustration of the data during the bottom time of the ISTA system, the salinity and temperature values are plotted against time. The images Fig. 8a,b characterize a situation comparable to that described above. In the time after the deployment no active fluid discharge was recorded, but after a few minutes another water mass entered and mixing occurred. The appearance of 'schlieren' are an indicator for discharged fluids in the ambient area of the instrument, which are transported laterally due to the bottom current. This effect was already recorded in the flume experiment as visible in Fig. 5b. An included funnel described in the following section was helpful to distinguish between lateral and vertical flows.

In contrast to earlier investigations where highly variable salinity depletions in the bottom water were observed (Bussmann and Suess, 1998), our CTD data show very small anomalies of salinity (a) $\Delta S = 0.045$ psu and temperature (b) $\Delta T = 0.1$°C. Nevertheless, with regard to the recorded video sequence, a significant correlation between these two detection methods is obvious. Salinity as well as temperature shows a well-defined signal in a second water mass. Even though the variation is small, a negative salinity and a positive temperature anomaly are visible. The resulting density decrease is calculated to be

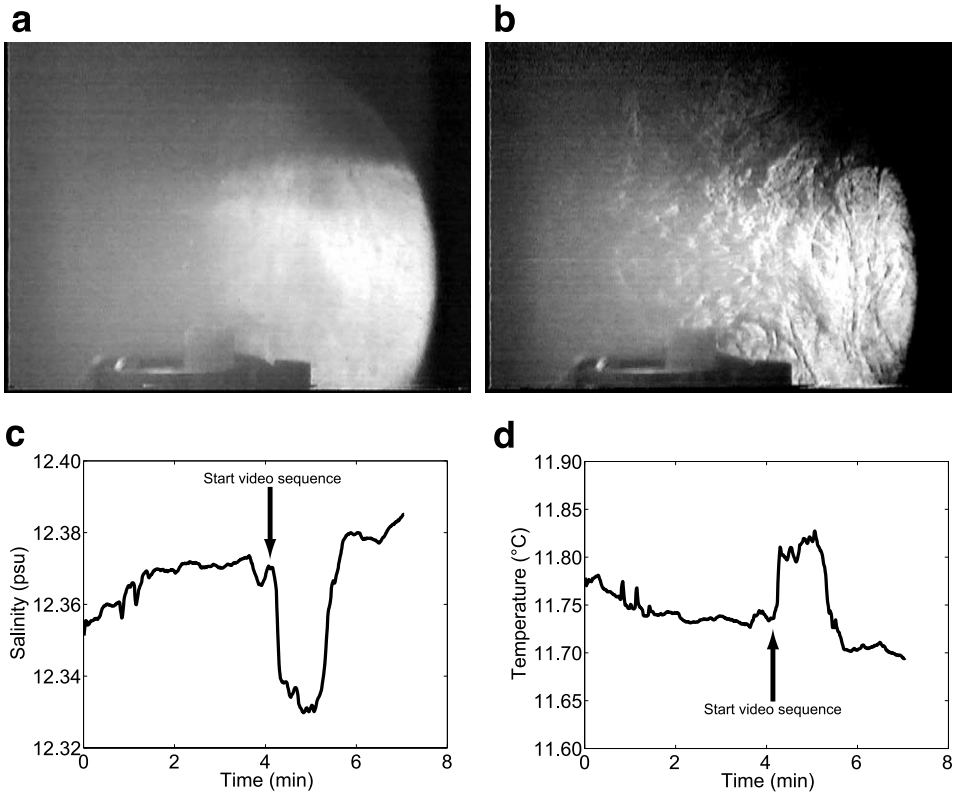

Fig. 8. Station 6, 7.9 m water depth. Screen shot (a) (6 cm in diameter) displays homogeneous bottom water. At a bottom current velocity of about 2 cm s^{-1}, the propagation of a discharged fluid can be seen (b). This phenomenon was also recorded in the corresponding CTD-data (c,d). (c) Salinity vs. time. (d) Temperature vs. time. In both diagrams the impact of a water mass from a fluid discharge site can be seen. The start of the video sequence is marked.

$\Delta\sigma_t = 0.049$. With respect to the smallest detectable difference of $\Delta\sigma_t = 0.023$ from the flume experiment, a good agreement between the laboratory test and the field deployment is thus established. The video sequence also confirms that the less dense fluid does not directly ascend upwards but rather is entrained in the turbulent bottom layer. At Stations 2 and 6, the transition of a homogeneous to a heterogeneous medium was recorded. Similar heterogeneous bottom water masses were observed at Stations 1, 3, 5. These seep influenced stations as seen on the map (Fig. 6; Table 1) lead to the outcome that a recognizable fluid discharge not only occurs in deep areas with close proximity to the pockmarks but also in shallower areas at the central ridge and the coastline. Especially in areas with little water depth and no obvious pockmark structures the ISTA represents an additional tool to detect fluid discharges.

3.1.2. Channeled groundwater discharge

For the next deployment, the inverted funnel described above was integrated into the optical pathway. This enabled the capture of discharged fluids and the channeling of outflow to a focal point. Deployments with this modification allow the characterization of the outflow activity from the base area of the funnel. Discharged fluids are amplified and more readily detectable against the lateral transported fluids from ambient seepages.

At Station 4 the instrument was deployed at 18.6 m water depth. Fig. 9a shows the discharge of fluids channeled by the inverted funnel. The exhaust port is visible at the base on the screen

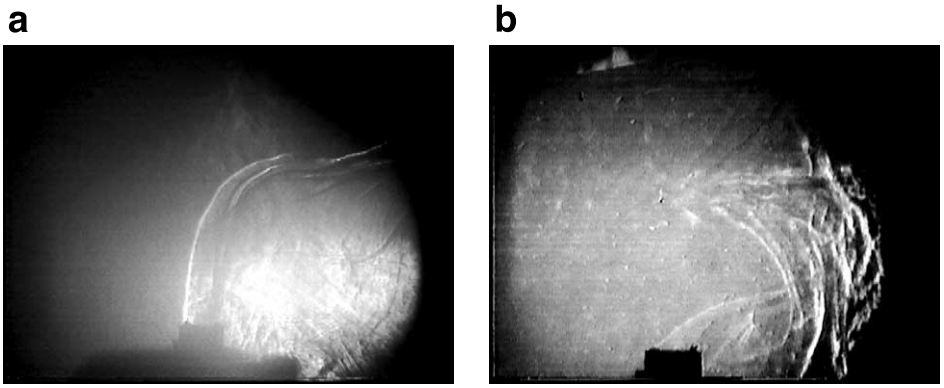

Fig. 9. Discharged groundwater is captured by an inverted funnel and channeled into the optical path way. (a) Station 4, 18.6 m water depth, horizontal image diameter is about 8 cm. (b) Station 2, 6.7 m water depth, horizontal image diameter is about 6 cm.

shot. A strong and continuous fluid flow was recorded. Fluids released outside the base of the funnel also appear as diffuse 'schlieren' objects in the background of the imaged funnel. At Station 2, where lateral transport of a discharged water mass was observed, it was possible to additionally record a fluid discharge from below channeled by the funnel at 6.7 m water depth (Fig. 9b). Compared to Station 4 the discharge is weaker and less clearly visible. Due to the enhanced bottom current the plume does not ascend vertically, instead it is deflected horizontally. Fluids which are discharged elsewhere outside the funnel and are transported laterally within the turbulent bottom layer also pass the field of view, as seen on the right hand side of this image.

3.2. Offshore test, hydrate ridge, Cascadia

The ISTA was tested and deployed under offshore conditions at the Cascadia continental margin (Fig. 10) during the TECFLUX (TECtonically-induced FLUXes) Expedition July/August 2000; RV *Sonne* Cruise 148.

The RV *Sonne* is equipped with a fiber-optic cable (Linke et al., 1994) and thus TV-guided deployment of the ISTA was possible. The unique deep-sea cold-vent setting is characterized by the occurrence of methane hydrate within deeper sediment layers as well as exposed at the sea floor (Suess et al., 1999). Due to plate convergence where the Juan de Fuca plate collides with the North American plate, thrusting and tectonic uplift take place. By this processes overpressured fluids and escape routes are developed. Along emerging faults fluids of differing salinity, generated by methane hydrate destabilization and formation, respectively, can escape from deeper layers and transport nutrients and other diluted material to the sediment–water interface. This process causes major transformations of the upper sediment layers and strongly affects the ecosystem at the seafloor.

Reduced chemical species, i.e. methane, hydrogen sulfide, and ammonia, trigger a massive growth of macro- and micro-organisms based on the anaerobic oxidation of methane (Boetius et al., 2000). For the main deployment sites, specific bacterial mats and clam fields were selected on the southern summit of Hydrate Ridge. The highest dewatering fluxes were expected here. Using the frame of a TV-guided multiple-corer (Barnett et al., 1984), the camera system was deployed on bacterial mat sites (Fig. 10). With the fiber-optical system, the video signal of the ISTA was available online for first interpretation. The videos showed immediately whether fluids were expelled and whether or not they were caught by the funnel and channeled upwards. These first results should be seen as a proof-of-concept because of the short deployment time. The ISTA was deployed at Stations 45 and 68 for 12 and 8 min, respectively. Only long term deployments with a time lapse control can visualize steady flow events. This

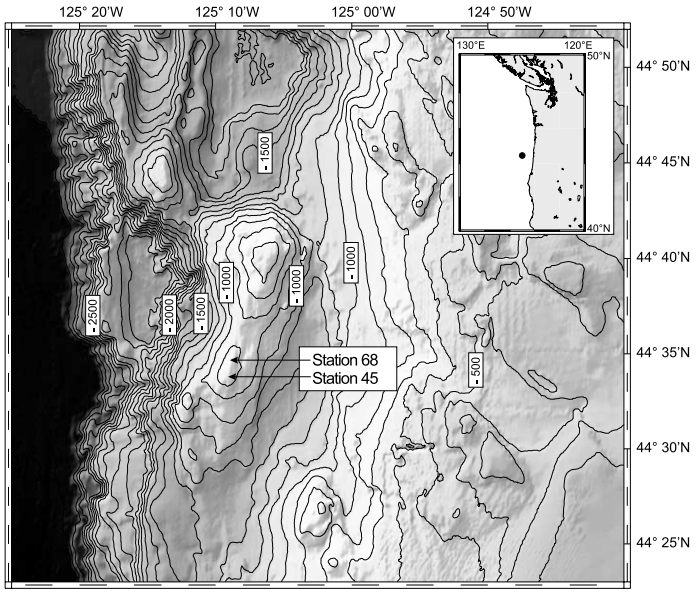

Fig. 10. Research site at the Cascadia continental margin off Oregon: ISTA was deployed at the southern summit of Hydrate Ridge at a water depth of approximately 800 m.

could only be realized with autonomous lander systems.

As an example, the two 'schlieren' images in Fig. 11 show diffusive fluid discharge that is only partly captured by the funnel. They do not look as clear as those obtained previously nor is the circular field of view fully realized. This is caused by difficulties during the installation of ISTA to the multi-corer. The system was installed into the frame, which caused tension on the camera frame and hence misalignment. As a consequence, the optical pathway was several millimeters out of focus. This problem has only been solved after the cruise with mechanical adaptations. Nevertheless, the reduced quality still recorded the mixing of two different water masses. In Fig. 11a, the exhaust port of the funnel is visible at the bottom of the image. Only the boundaries of the discharged fluid are visible but inside the plume resuspended particles following the up-

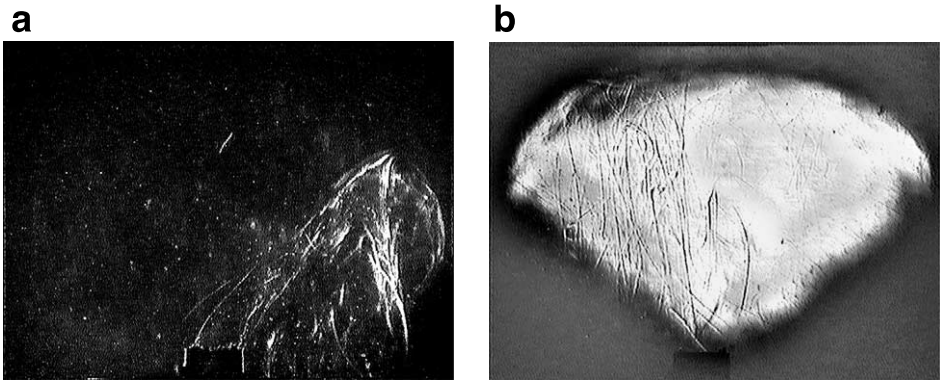

Fig. 11. (a) Station 45. Discharging diffuse fluids are captured and focused by an inverted funnel. (b) Station 68. There is no flow through the funnel, but discharged fluids adjacent to it, which were not captured, are visible. The horizontal diameter of the images is about 6 cm.

ward flow are visible. A direct fluid discharge through the funnel is not visible at Station 68 (Fig. 11b), but thin 'schlieren' objects transported laterally due to a bottom current are visible.

4. Discussion and conclusions

A new way of investigating submarine water discharges such as cold seeps by optical means is presented here. Vigorous hot water discharge commonly observed at the hot vents is easy to observe with common camera techniques. However, even in these areas, moderate diffuse fluxes cannot be detected. Common techniques are not sufficiently sensitive to detect very slow discharges. The 'schlieren' technique applied here is far more sensitive in detecting heterogeneous water masses than other techniques. The seep-meter like instruments from Lee (1977), Linke et al. (1994), and Tryon et al. (2001) are designed to quantify the fluid flow from the sediment–water interface, where as the newly described 'schlieren' technique is developed to visualize the fluid flux. It was not only possible to discover direct fluid discharges, but also to survey the dispersion of discharged fluids into the ambient bottom water. It is known that the discharged groundwater in the Eckernförde Bay is depleted in salinity and, thus, a strong outflux can reduce the salinity of the ambient bottom water. Bussmann and Suess (1998) measured a range of salinities of the adjacent water column from 18.3 to 2.9 psu. These values represent a highest dilution of $\Delta S = 15.4$ psu. Other measurements of the same study yielded less or non-detectable dilutions. By using the 'schlieren' technique with a CTD simultaneously, it could be demonstrated that the optical technique was sensitive enough to visualize density variations of $\Delta\sigma_t = 0.049$ in heterogeneous water masses. These were caused by a salinity anomaly of $\Delta S = 0.045$ psu and a temperature anomaly of $\Delta T = 0.1$°C. The simultaneous use of a CTD and the ISTA enables researchers to characterize the mixing processes of a discharged fluid with the ambient bottom water. Only the video recordings discover whether the fluids are discharged from the sediment–water interface or transported from the near proximity. In addition, even small-scale mixing processes, such as bottom boundary layer eddies, could be analyzed. The observed in-situ phenomena are well comparable with the performed flume experiments in respect to flow pattern and sensitivity. Smallest density variations of $\Delta\sigma_t = 0.023$ were visualized and the comparable flow pattern demonstrated that analog experiments within the GEOMAR seawater flume were feasible to describe natural fluid discharges.

With echo-sounder systems, pockmarks are detectable and are explained by freshwater discharge combined with particle resuspension (Sauter et al., 2001). Further investigations, using the ISTA system, were done inside and outside these pockmarks, highlighting new sources of fluid discharge in the Eckernförde Bay. With regard to the discovery of active vent sites and the survey of the distribution of the fluids, the ISTA instrument opens up new possibilities to better achieve this task. The investigation of active vent sites with the use of an inverted funnel provides new possibilities for the quantification of flow and areal estimates. Currently active fluid discharge in the Eckernförde Bay was observed at two stations (Fig. 6, Nos. 2, 4). The channeled flow through the funnel is an indication of the high intensity of the venting activity. The strongest discharge was detected at Station 4 with continuous and vigorous fluid flow. Both stations are identified as new vent sites not previously known and, especially Station 2, differ in depth (6.7 m) from most known seep locations. The tracking of resuspended particles within the ascending jet should be performed in further deployments to quantify the flow rate. The ratio between the exhaust port and base area is known to be 0.26 cm^2 to 102.07 cm^2. At this stage an accurate quantification was not possible due to an insufficient resolution of the visible outflow. Nevertheless, a rough estimate of the outflow velocity through the exhaust provided values in order of 1 cm s^{-1} but a flux estimate is too speculative for this data.

The universal capability and wide applicability of the new technique was demonstrated with its successful offshore test deployment. Minor mechanical problems reduced the quality of the im-

age but the deployment was satisfactory and documented the highly dynamic and small-scale fluid activity. For future deployments a longer deployment with an autonomous lander system would be feasible. The first cabled test deployments where too short in time to exclude artifical fluxes due to the disturbances of the deployed instrument. But as described above, the 'schlieren' technique is sensitive to the smallest density variations in heterogeneous water masses. Thus, it is likely that nearly all kinds of discharged fluids can be visualized with this optical instrument. The occurrence of biogeochemical processes within the sediments causes an alteration of the chemical composition. It is known that the destabilization of methane hydrates releases pure water (Suess et al., 1999) and during the reversed mechanism of hydrate formation a positive chloride anomaly due to salt exclusion occurs (Haeckel et al., in prep.). A fluid flow with increased chloride concentration is also found in brines such as those of the Mediterranean (Wallmann et al., 1997b). For these seep sites it is likely that fluid discharges could be detected with the 'schlieren' technique as well. Limitations of this approach are predominantly the general conditions. As recognized high particulate matter reduces the quality of the records which was most obvious within the pockmark locations. Bottom currents with speeds of more than 5 cm s^{-1} also reduce the quality of the video record. A frame with current shields could solve this weakness.

Boundary layers within the water column such as pycnoclines or the benthic boundary layer are regions of enhanced mixing and of particular importance in investigating the distribution of fluids and particles. So far, visualization of these processes has only been possible by applying tracers such as dye (O'Riordan et al., 1993). Laboratory and field experiments demonstrated the ability of the new optical application to visualize small-scale mixing processes without the help of dye or any other tracers. Other possible fields of application are phenomena such as salt fingering below the outflow of Mediterranean Water into the Atlantic which can make a significant contribution to vertical mixing within the oceans (Williams, 1975).

Using the multi-corer frame with the fiber-optic cable aboard RV *Sonne*, video-guided ISTA-deployment was possible. Dampers will be inserted between the multi-corer frame and the ISTA in further deployments to prevent tension on the instrument's frame. For a deep-sea operable optical instrument, this new system is relatively low-priced and applicable for numerous environments being investigated using different platforms, e.g. small or large research vessels, permanent towers etc. This new technique is certain to discover new groundwater seeps and cold vents and eventually will be an aid in quantifying fluid discharge rates at different cold seep settings.

Acknowledgements

Helpful reviews of this manuscript by Eberhard Sauter and Mike Tryon are gratefully acknowledged. We are grateful to the excellent technical support of Asmus Petersen (KUM). In particular, we thank Peter Linke for his encouragement as chief scientist, as well as Frank Appel and Bernhard Bannert for their technical help during Cruise SO-148/1. We greatly appreciate the support at sea by the captains and crews of RV *Littorina* and RV *Sonne*. Gregor Rehder is gratefully acknowledged for his detailed review. This study was funded by the Deutsche Forschungsgemeinschaft, the graduate school 'Dynamics of Global Cycles' (GRK-171) at the Christian-Albrechts-Universität of Kiel, the Land Schleswig-Holstein, and the Federal Ministry for Education and Research; Fz: 03GO 148.

References

Aharon, P., 1994. Geology and biology of modern and ancient submarine hydrocarbon seeps and vents; an introduction. Geo Mar. Lett. 14, 69–73.

Albert, D.B., Martens, C.S., Alperin, M.J., 1998. Biogeochemical processes controlling methane in gassy coastal sediments – Part 2. Groundwater flow control of acoustic turbidity in Eckernförde Bay. Cont. Shelf Res. 18, 1771–1793.

Barnett, P.R.O., Watson, J., Conelly, D., 1984. A multiple corer for taking virtually undisturbed samples from shelf, bathyal and abyssal sediments. Oceanol. Acta 7, 399–408.

Boetius, A., Ravenschlag, K., Schubert, C.J., Rickert, D., Widdel, F., Gieseke, A., Amann, R., Jørgensen, B.B., Witte,

U., Pfannkuche, O., 2000. A marine microbial consortium apparently mediating anaerobic oxidation of methane. Nature 407, 623–626.

Burnett, W.C., Taniguchi, M., Oberdorfer, J., 2001. Measurement and significance of the direct discharge of groundwater into the coastal zone. J. Sea Res. 46, 109–116.

Bussmann, I., Dando, P.R., Niven, S.J., Suess, E., 1999. Groundwater seepage in the marine environment: Role for mass flux and bacterial activity. Mar. Ecol. Prog. Ser. 178, 169–177.

Bussmann, I., Suess, E., 1998. Groundwater seepage in Eckernförde Bay (Western Baltic Sea): Effect on methane and salinity distribution of the water column. Cont. Shelf Res. 18, 1795–1806.

Cable, J.E., Burnett, W.C., Chanton, J.P., Weatherly, G.L., 1996. Estimating groundwater discharge into the northeastern Gulf of Mexico using radon-222. Earth Planet. Sci. Lett. 144, 591–604.

Carson, B., Suess, E., Strasser, J.C., 1990. Fluid flow and mass flux determinations at vent sites on the Cascadia Margin accretionary prism. J. Geophys. Res. 95, 8891–8897.

Converse, C.H., Williams, A.J., Fucile, P.D., Schmitt, R.W., 1986. A free ocean vehicle to measure optical microstructure. Curr. Pract. New Tech. Ocean Eng. 11, 341–345.

Corbett, D.R., Chanton, J., Burnett, W., Dillon, K., Rutkowski, C., Fourqurean, J.W., 1999. Patterns of groundwater discharge into Florida Bay. Limnol. Oceanogr. 44, 1045–1055.

Corliss, J.B., Dymond, J., Gordon, L.I., Edmond, J.M., von Herzen, R.P., Ballard, R.D., Green, K., Williams, D., Bainbridge, A., Crane, K., van Andel, T.H., 1979. Submarine thermal springs on the Galápagos Rift. Science 203, 1073–1083.

Dietrich, G., Kalle, K., Krauss, W., Siedler, G., 1975. Allgemeine Meereskunde, 3rd ed. Borntraeger, Berlin.

Fofonoff, N.P., Millard, R.C., 1983. Algorithms for computation of fundamental properties of seawater. Unesco Tech. Pap. Mar. Sci. 44, 53.

Haeckel, M., Suess, E., Wallmann, K., Rickert, D., in prep. Rising methane gas-bubbles form massive methane layers at the sea floor.

Hovland, M., 1992. Hydrocarbon seeps in Northern marine waters – Their occurrence and effects. Palaios 7, 376–382.

Hovland, M., Judd, A.G., 1988. Seabed Pockmarks and Seepages: Impact on Geology, Biology and the Marine Environment. Graham and Trotman, London.

Johannes, R.E., 1980. The ecological significance of the submarine discharge of groundwater. Mar. Ecol. Prog. Ser. 3, 365–373.

Johannes, R.E., Hearn, C.J., 1985. The effect of submarine groundwater discharge on nutrient and salinity regimes in a coastal lagoon off Perth, Western Australia. Est. Coast. Shelf Sci. 21, 789–800.

Karpen, V., 1999. Experimentelle Untersuchngen von Austauschprozessen in der Sediment–Wasser-Grenzschicht. Diplomarbeit, Christian-Albrechts-Universität, Kiel.

Khandriche, A., Werner, F., 1995. Freshwater induced pockmarks in Bay of Eckernfoerde, Western Baltic. Proceedings of the Third Marine Geological Conference 'The Baltic', pp. 155–164.

Kulm, L.D., Suess, E., Moore, J.C., Carson, B., Lewis, B.T., Ritger, S.D., Kadko, D.C., Thornburg, T.M., Embley, R.W., Rugh, W.D., Massoth, G.J., Langseth, M.G., Cocharane, G.R., Scamman, R.L., 1986. Oregon subduction zone: Venting, fauna and carbonates. Science 231, 561–566.

LaRoche, J., Nuzzi, R., Waters, M., Wyman, K., Falkowski, P., Wallace, D.W.R., 1997. Brown Tide blooms in Long Island coastal waters linked to interannual variability in groundwater flow. Glob. Change Biol. 3, 397–410.

Lee, D.R., 1977. A device for measuring seepage flux in lakes and estuaries. Limnol. Oceanogr. 22, 140–147.

Linke, P., Suess, E., Torres, M., Martens, V., Rugh, W.D., Ziebis, W., Kulm, L.D., 1994. In situ measurement of fluid flow from cold seeps at active continental margins. Deep-Sea Res. I 41, 721–739.

Millard, R.C., Seaver, G., 1990. An index of refraction algorithm for seawater over temperature, pressure, salinity, density, and wavelength. Deep-Sea Res. I 37, 1909–1926.

Moore, W.S., 1996. Large groundwater inputs to coastal waters revealed by ^{226}Ra enrichments. Nature 380, 612–614.

O'Riordan, C.A., Monismith, S.G., Koseff, J.R., 1993. A study of concentration boundary-layer formation over a bed of model bivalves. Limnol. Oceanogr. 38, 1712–1729.

Paull, C.K., Hecker, B., Commeau, R., Freeman-Lynde, R.P., Neumann, C., Corso, W.P., Golubic, S., Hook, J.E., Sikes, E., Curray, J., 1984. Biological communities at the Florida escarpment resemble hydrothermal vent taxa. Science 226, 965–967.

Sauter, E.J., Laier, T., Andersen, C.E., Dahlgaard, H., Schlüter, M., 2001. Sampling of sub-seafloor aquifers by a temporary well for CFC age dating and natural tracer investigations. J. Sea Res. 46, 177–185.

Schardin, H., 1942. Die 'schlieren'verfahren und ihre Anwendungen. Ergeb. Exakten Nat.wiss. 20, 304–405.

Seaver, G.A., 1985. The index of refraction to specific volume relation for sea water – A linearized equation of state. J. Phys. Oceanogr. 15, 1339–1343.

Settles, G.S., 2001. 'Schlieren' and Shadowgraph Techniques: Visualizing Phenomena in Transparent Media. Springer, Berlin.

Sonrel, L., 1868. Le fond de la mer. Hachette, Paris.

Springer, B., Friedrichs, M., Graf, G., Nittikowski, J., Queisser, W., 1999. A high-precision current measurement system for laboratory ume systems: A case study around a circular cylinder. Mar. Ecol. Prog. Ser. 183, 305–310.

Suess, E., Carson, B., Ritger, S.D., Moore, J.C., Jones, M.L., Kulm, L.D., Cochrane, G.R., 1985. Biological communities at vent sites along the subduction zone off Oregon. Bull. Biol. Soc. Wash. 6, 475–484.

Suess, E., Linke, P., 2002. Der Ozean unter dem Meeresboden: Kalte Quellen als Oasen der Tiefsee. In: Wefer, G. (Ed.), Expedition Erde, Universität Bremen.

Suess, E., Torres, M.E., Bohrmann, G., Collier, R.W., Greinert, J., Linke, P., Rehder, G., Trehu, A., Wallmann, K.,

Winckler, G., Zuleger, E., 1999. Gas hydrate destabilization: Enhanced dewatering, benthic material turnover and large methane plumes at the Cascadia convergent margin. Earth Planet. Sci. Lett. 170, 1–15.

Thomsen, L., Jähmlich, S., Graf, G., Friedrichs, M., Wanner, S., Springer, B., 1996. An instrument for aggregate studies in the benthic boundary layer. Mar. Geol. 135, 153–157.

Töpler, A., 1866. Über die Methode der 'schlieren'beobachtung als mikroskopisches Hilfsmittel, nebst Bemerkungen zur Theorie der schiefen Beleuchtung. Poggendorf's Ann. Phys. Chem. 127, 556–580.

Töpler, A., 1867. Optische Studien nach der Methode der 'schlieren'beobachtung. Poggendorf's Ann. Phys. Chem. 131, 33–55.

Tryon, M., Brown, K., 2001. Complex flow patterns through Hydrate Ridge and their impact on seep biota. Geophys. Res. Lett. 28, 2863–2866.

Tryon, M., Brown, K., Dorman, L., Sauter, A., 2001. A new benthicaqueous flux meter for very low to moderate discharge rates. Deep-Sea Res. I 48, 2121–2146.

Valiela, I., Costa, J., Foreman, K., Teal, J.M., Howes, B.L., Aubrey, D.G., 1990. Transport of groundwater-borne nutrients from watersheds and their effects on coastal waters. Biogeochemistry 10, 177–197.

Wallmann, K., Linke, P., Suess, E., Bohrmann, G., Sahling, H., Schlüter, M., Dählmann, A., Lammers, S., Greinert, J., von Mirbach, N., 1997a. Quantifying fluid flow, solute mixing, and biogeochemical turnover at cold vents of the eastern Aleutian subduction zone. Geochim. Cosmochim. Acta 61, 5209–5219.

Wallmann, K., Suess, E., Westbrook, G.H., Winckler, G., Cita, M.B., 1997b. Salty brines on the Mediterranean sea oor. Nature 387, 31–32.

Werner, F., 1978. Depressions in mud sediments (Eckernfoerde Bay, Baltic Sea), related to sub-bottom and currents. Meyniana 30, 99–104.

Whiticar, M.J., 2002. Diagenetic relationships of methanogenesis, nutrients, acoustic turbidity, pockmarks and freshwater seepages in Eckernförde Bay. Mar. Geol. 182, 29–53.

Whiticar, M.J., Werner, F., 1981. Pockmarks: submarine vents of natural gas or freshwater seeps? Geo Mar. Lett. 1, 193–199.

Williams, A.J., 1975. Images of ocean microstructure. Deep-Sea Res. I 22, 811–829.

Zektser, I.S., Loaiciga, H.A., 1993. Groundwater fluxes in the global hydrologic cycle: Past, present and future. J. Hydrol. 144, 405–427.